The Journal of Chemical Physics

Excitonic coupling effect on the circular dichroism spectrum of sodium-pumping rhodopsin KR2

Cite as: J. Chem. Phys. **153**, 045101 (2020); https://doi.org/10.1063/5.0013642
Submitted: 13 May 2020 . Accepted: 05 July 2020 . Published Online: 22 July 2020

Kazuhiro J. Fujimoto, and Keiichi Inoue

The Journal of Chemical Physics ARTICLE scitation.org/journal/jcp

Excitonic coupling effect on the circular dichroism spectrum of sodium-pumping rhodopsin KR2

Cite as: J. Chem. Phys. 153, 045101 (2020); doi: 10.1063/5.0013642
Submitted: 13 May 2020 • Accepted: 5 July 2020 •
Published Online: 22 July 2020

Kazuhiro J. Fujimoto[1,a)] and Keiichi Inoue[2]

AFFILIATIONS

[1]Institute of Transformative Bio-Molecules (WPI-ITbM), Nagoya University, Furocho, Chikusa, Nagoya 464-8601, Japan
[2]The Institute for Solid State Physics, The University of Tokyo, 5-1-5 Kashiwanoha, Kashiwa-shi, Chiba 277-8581, Japan

[a)]**Author to whom correspondence should be addressed:** fujimotok@chem.nagoya-u.ac.jp

ABSTRACT

We investigate the role of excitonic coupling between retinal chromophores of *Krokinobacter eikastus* rhodopsin 2 (KR2) in the circular dichroism (CD) spectrum using an exciton model combined with the transition density fragment interaction (TDFI) method. Although the multimer formation of retinal protein commonly induces biphasic negative and positive CD bands, the KR2 pentamer shows only a single positive CD band. The TDFI calculation reveals the dominant contribution of the Coulomb interaction and negligible contributions of exchange and charge-transfer interactions to the excitonic coupling energy. The exciton model with TDFI successfully reproduces the main features of the experimental absorption and CD spectra of KR2, which allow us to investigate the mechanism of the CD spectral shape observed in the KR2 pentamer. The results clearly show that the red shift of the CD band is attributed to the excitonic coupling between retinal chromophores. Further analysis reveals that the weak excitonic coupling plays a crucial role in the shape of the CD spectrum. The present approach provides a basis for understanding the origin of the KR2 CD spectrum and is useful for analyzing the mechanism of chromophore–chromophore interactions in biological systems.

I. INTRODUCTION

Circular dichroism (CD) is defined as the difference between the absorptions of left and right circularly polarized light, which is widely used in determining the absolute configuration of a molecule.[1] CD measurements have also been used as a sensitive tool for analyzing chromophore–chromophore and chromophore–protein interactions.[2–7]

Excitonic coupling (or electronic coupling), which is an intermolecular interaction between different electronic states, is known to affect the shape of the CD spectrum, and this phenomenon is called exciton-coupled CD (ECCD).[1,8] ECCD is characterized by two large CD bands with opposite signs (Cotton effect), which strongly reflects the intermolecular conformation between two or more chromophores.

Several theoretical methods have been proposed for calculating the ECCD spectrum.[9–11] Among them, the matrix method[12–16] (exciton model) based on the coupled oscillator method[17,18] and the Frenkel exciton model[19] is commonly used for the CD calculations because of its simplicity. In this method, excitonic coupling corresponds to the off-diagonal elements of the Hamiltonian matrix, so that an accurate description of excitonic coupling plays a vital role in the CD calculation.

To accurately calculate the excitonic coupling, many theoretical methods have been developed.[20–34] One of the authors developed a transition density fragment interaction (TDFI) method.[35–37] The TDFI method can describe not only excitonic Coulomb coupling but also exchange coupling.[36] Furthermore, in combination with the transfer-integral method (TDFI-TI),[36] the TDFI method can calculate the contribution of the charge-transfer (CT) interaction to the excitonic coupling. These advantages of the TDFI method allow for a more accurate description and detailed analysis of excitonic coupling, compared to other methods.[38] In our previous studies, the exciton model combined with TDFI was applied to

photochemical and photobiological systems, such as a retinal dimer,[38] xanthorhodopsin (XR),[39] and tetracene crystal,[40] and successfully reproduced the characteristic absorption and CD spectra observed in the experiments.

This study focuses on the role of excitonic coupling in spectral properties of *Krokinobacter eikastus* rhodopsin 2 (KR2),[41–43] a retinal-based light-driven outward sodium pump. KR2 is the first non-protonic cation pumping rhodopsin, and its transport mechanism is completely different from proton pumping rhodopsins.[42,44,45] It has also received much attention in the field of neuroscience because of its potential as an optogenetic tool.[42,46,47] In general, a retinal protein shows a single positive CD band in the retinal absorption wavelength when it is a monomer, but the formation of a multimer brings about a significant change in the CD spectral shape.[3,7,48] In the case of bacteriorhodopsin, trimer formation induces biphasic negative and positive CD bands, which is considered ECCD.[3,7] KR2 also forms a pentamer in the membrane environment, so that the emergence of the biphasic CD was expected. However, the measured KR2 CD spectrum exhibited only a single positive band.[49] This may suggest that, unlike other retinal proteins, excitonic coupling does not affect the CD spectral shape of the KR2 pentamer. On the other hand, the CD spectrum of KR2 showed a spectral red shift in the positive band compared to the absorption band, suggesting that multimeric interactions may contribute to the CD spectrum. These facts raise the question of whether the unexpected CD spectrum of the KR2 pentamer is due to excitonic coupling. However, since no detailed analysis of the KR2 CD spectrum has been performed, the exact origin remains unclear.

The purpose of this study is to clarify how excitonic coupling affects the CD spectrum of the KR2 pentamer. To this end, we perform the CD spectral calculations using the exciton model with TDFI. The calculated spectrum is compared to the experimental one. Based on the successful reproduction of the KR2 CD spectrum, the underlying molecular mechanism is explored.

II. THEORY

We briefly explain the CD calculation based on the exciton model combined with TDFI. The details of the TDFI method are described in Refs. 36, 37, and 40.

The total Hamiltonian for N molecules is given by

$$\hat{H} = \sum_{i}^{N} \hat{H}_i + \sum_{i}^{N} \sum_{j>i}^{N} \hat{V}_{ij}, \tag{1}$$

where $\hat{H}$ is the local Hamiltonian for molecule i, and $\hat{V}$ is the excitonic interaction between different molecules i and j. In the exciton model, we consider the basis represented by the direct product of the electronic states for N molecules,

$$\left|\Phi_i^{\mathrm{e}}\right\rangle = \left|\varphi_1^{\mathrm{g}} \cdots \varphi_i^{\mathrm{e}} \cdots \varphi_N^{\mathrm{g}}\right\rangle, \tag{2}$$

where φ_i^a denotes the state a [a = ground state (g) or excited state (e)] for molecule i. For simplicity, let us consider only two electronic states for molecules i and j (i.e., $N = 2$). Then, the basis becomes

$$\begin{aligned} |\Phi_1\rangle &= \left|\varphi_i^{\mathrm{e}} \cdot \varphi_j^{\mathrm{g}}\right\rangle, \\ |\Phi_2\rangle &= \left|\varphi_i^{\mathrm{g}} \cdot \varphi_j^{\mathrm{e}}\right\rangle. \end{aligned} \tag{3}$$

Using Eq. (3), the 2 × 2 Hamiltonian matrix is described as

$$\mathbf{H} = \begin{pmatrix} E_i & V_{ij} \\ V_{ji} & E_j \end{pmatrix}. \tag{4}$$

Here, the diagonal element E_i represents the electronic excitation energy of molecule i. The off-diagonal element V_{ij} is the excitonic coupling between molecules i and j. In the TDFI method, the excitonic coupling is described as[36]

$$\begin{aligned} V_{ij} &= \sum_{\nu,\mu\in i} \sum_{\lambda,\sigma\in j} P_{\nu\mu}^{i} P_{\lambda\sigma}^{j} \left[(\mu\nu|\sigma\lambda) - \frac{1}{2}(\mu\lambda|\sigma\nu) \right] \\ &\equiv V_{\mathrm{Coul}} + V_{\mathrm{Exch}}, \end{aligned} \tag{5}$$

where $P_{\nu\mu}^{i}$ is a one-electron transition density matrix for molecule i, and $(\mu\nu|\sigma\lambda)$ is an atomic orbital two-electron integral. The first and second terms of Eq. (5) correspond to excitonic coupling of the Coulomb (V_{Coul}) and exchange (V_{Exch}) interactions between two molecules, respectively.

The Kth exciton state (i.e., the excited state for the total system) is represented by a linear combination of Eq. (3),

$$|\Psi_K\rangle = \sum_{l} C_{lK} |\Phi_l\rangle. \tag{6}$$

To determine the expansion coefficients C_{lK}, the Hamiltonian matrix $\mathbf{H}$ [Eq. (4)] is numerically diagonalized with the Löwdin symmetric orthogonalization method.[50] Following this procedure, the energies of the exciton states E_K are also obtained. E_K directly corresponds to the excitation energy of the Kth exciton state because the ground state energy is set to be zero (i.e., $E_0 = 0$) in the present scheme.

Using the expansion coefficients C_{lK} [Eq. (6)], velocity transition dipole moments and magnetic transition dipole moments for the non-interacting system are transformed to the ones for the interacting system,[38]

$$\nabla'_K = \sum_{l} C_{lK} \nabla_l, \tag{7a}$$

$$\mathbf{m}'_K = \sum_{l} C_{lK} \mathbf{m}_l. \tag{7b}$$

Using these moments, the rotational strength of the Kth exciton state is obtained as

$$R_K = \frac{\mathrm{Im}\left(\nabla'_K \cdot \mathbf{m}'_K\right)}{E_K}. \tag{8}$$

Finally, the CD spectrum is calculated as

$$\Delta\varepsilon(E) \propto \sum_{K} \frac{R_K E_K}{\sqrt{2\pi}\sigma} \exp\left[-\frac{(E - E_K)^2}{2\sigma^2} \right], \tag{9}$$

where σ denotes the standard deviation of the Gaussian distribution.

III. COMPUTATIONAL DETAILS

The atomic coordinates of KR2 were taken from the crystal structure (PDB: 4XTO).[43] This structure was optimized with

the hybrid quantum mechanics/molecular mechanics (QM/MM) method,[51] in which density functional theory (DFT)[52] with the B3LYP functional[53] and the AMBER99 force field[54] were employed for the QM and MM atoms, respectively. The excitation energies and the transition densities were obtained with the density fragment interaction (DFI) method,[55] in which the symmetry-adapted cluster-configuration interaction (SAC-CI) method[56] and time-dependent DFT[57] with the CAM-B3LYP functional[58] (TD-CAM-B3LYP) were employed for the QM atoms. The protein electrostatic effect was described with the MM atoms represented by the AMBER99 force field.[54] A frozen core approximation to 1*s* core orbitals was employed in the SAC-CI and TD-CAM-B3LYP calculations. The split valence double-ζ plus polarization basis set (6-31G*) was used for all QM atoms. The retinal chromophore with the side chain of Lys255 and its counterion Asp116 were described as the QM atoms. The C_β–C_γ bond of Lys255 and the C_α–C_β bond of Asp116 were cut as the QM/MM boundary, and those were capped with hydrogen.[59] The excitonic coupling values were obtained with the TDFI method. A standard deviation of 0.18 eV was used in the spectral calculations [Eq. (9)]. The QM/MM geometry optimization and the DFI/TDFI computations were carried out with TINKER4.2[60] interfaced with the Gaussian09 program package[61]

IV. RESULTS

We first performed excited state calculations for the KR2 monomer. The structures used for the calculations are shown in Fig. 1(a). Table I summarizes the excitation energies, oscillator strength, and rotational strength obtained with the SAC-CI and TD-CAM-B3LYP methods. In both SAC-CI and TD-CAM-B3LYP calculations, the first excited states had large oscillator strength and were characterized as π–π* excitation from the highest occupied molecular orbital (HOMO) to the lowest unoccupied molecular orbital (LUMO). The excitation energies obtained with the SAC-CI and TD-CAM-B3LYP methods were 2.33 eV and 2.82 eV, respectively. It is noted that there is no experimental value for the excitation energy of the KR2 monomer. However, considering the experimental result for the KR2 pentamer (2.37 eV[41]), the SAC-CI excitation energy seemed to be close to the experimental value. Using the SAC-CI values, we also calculated absorption and CD spectra for the KR2 monomer. As shown in Fig. 2(a), the calculated absorption spectrum showed a band at 532 nm (2.33 eV), while the calculated CD spectrum [Fig. 2(b)] also showed a positive band at 532 nm (2.33 eV). Therefore, the peak position of the CD band [Fig. 2(b)] was the same as that of the absorption band for the KR2 monomer [Fig. 2(a)]. These results showed that the monomer calculation does not reproduce the red-shifted CD band observed in the experiment [Fig. 2(d)].[49] The positive CD band came from positive rotational strength (139×10^{-40} cgs), which was consistent with the retinal CD spectra obtained in our previous studies.[38,39]

Next, the TDFI calculations were applied to the retinal chromophores for calculating the excitonic coupling values. Here, we considered the retinal electronic transition between the ground and the first excited states. Table I also summarizes the calculated excitonic coupling values. The SAC-CI and TD-CAM-B3LYP calculations gave excitonic coupling values of 25.1 cm^{-1} and 35.8 cm^{-1}, respectively. The magnitudes of these excitonic coupling values were much smaller than that of XR (227 cm^{-1}),[39] indicating weaker interchromophore interactions for KR2. This can be understood from the protein structure of KR2. As shown in Fig. 1(b), the intermolecular N_ζ–N_ζ distance between retinal chromophores was ~25 Å. This intermolecular distance was much larger than the carotenoid–retinal distance in XR (~13 Å),[35] which resulted in the smaller excitonic coupling than that of XR. This result indicates that excitation energy transfer (EET) between the retinal chromophores in KR2 is less likely to occur than the EET between the carotenoid and retinal in XR.[62–64]

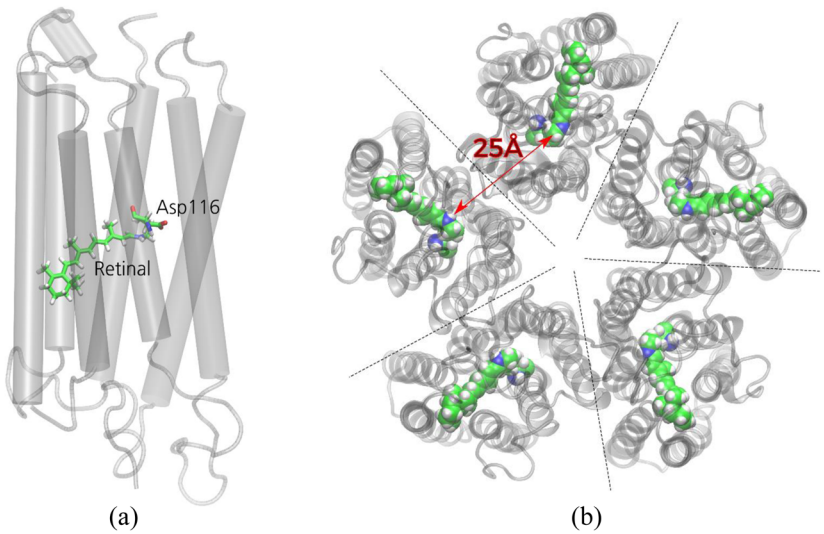

FIG. 1. Optimized structure of KR2. (a) Monomer and (b) pentamer. In (b), the intermolecular distance of 25 Å is shown.

TABLE I. Excitation energies, excitonic coupling energies, oscillator strength, and rotational strength of KR2.

		V (cm^{-1})[b]				
	E_{ex}[a] (eV)	Coulomb	Exchange	CT	f[c] (a.u.)	R[d] (10^{-40} cgs)
SAC-CI	2.33	25.1 (25.0)[e]	0.0	0.0	0.94	139
TD-CAM-B3LYP	2.82	35.8 (37.9)[e]	0.0	0.0	1.97	148

[a]Excitation energy for the KR2 monomer.
[b]Excitonic coupling energy obtained with the TDFI method.
[c]Oscillator strength for the KR2 monomer.
[d]Rotational strength for the KR2 monomer.
[e]Data calculated with the TrESP method.

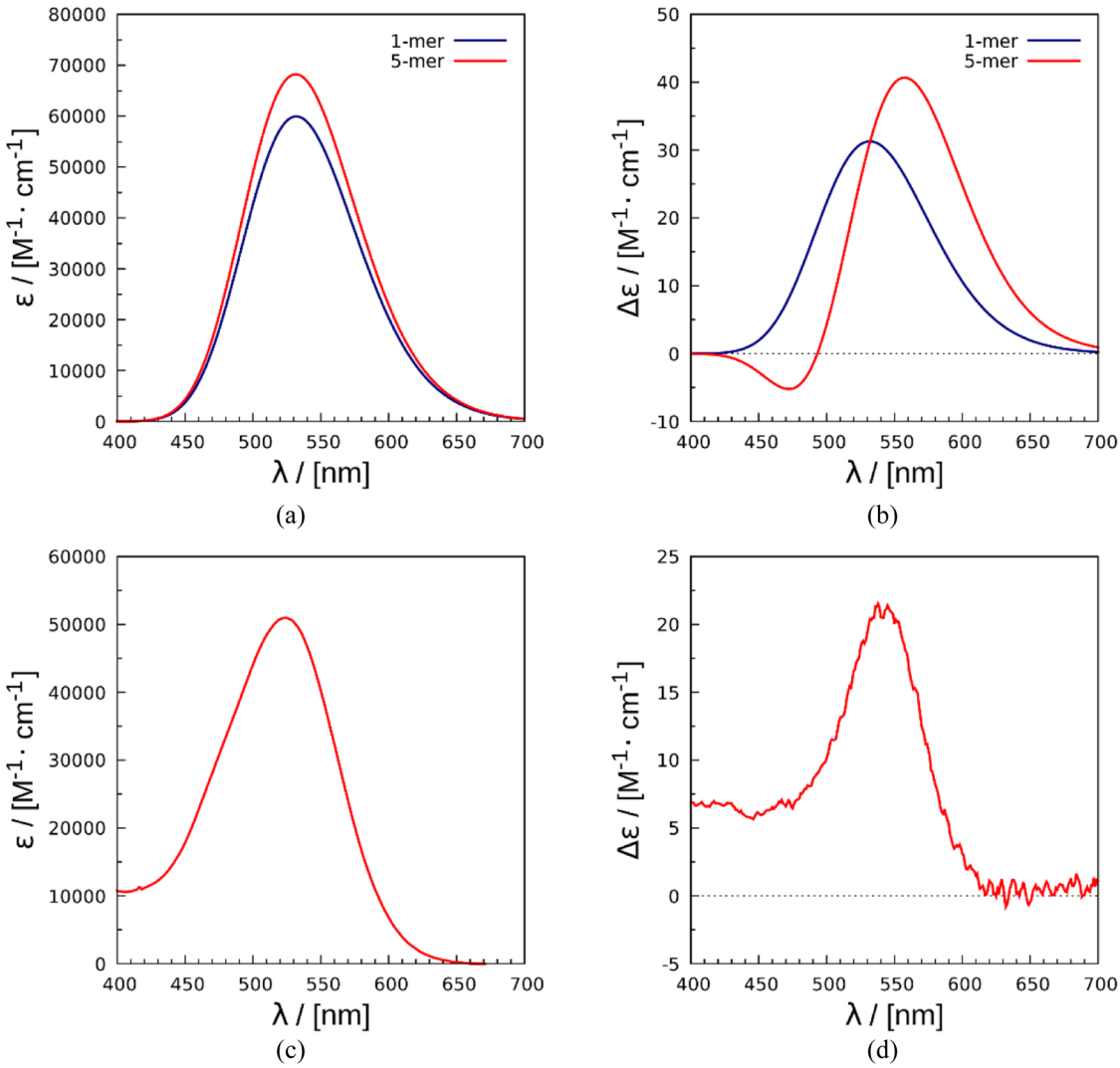

FIG. 2. Theoretical and experimental spectra of KR2. (a) Theoretical absorption, (b) theoretical CD, (c) experimental absorption of the KR2 pentamer (from Ref. 41), and (d) experimental CD of the KR2 pentamer (from Ref. 49). In (a) and (b), the values in the pentamer spectra are given per monomer.

We also examined each contribution to excitonic coupling in terms of Coulomb, exchange, and CT interactions. The CT interactions (i.e., indirect coupling[65]) were calculated with the TDFI-TI method,[36,37] where the contributions from retinal HOMO − 1, HOMO, LUMO, and LUMO + 1 were considered. As also listed in Table I, the Coulomb interaction was calculated to be 25.1 cm^{-1}, while exchange and CT interactions were 0.0 cm^{-1}. Therefore, the main contribution to excitonic coupling was found to be the Coulomb interaction. This result was also understood from the protein structure of KR2. The large inter-chromophore distance reduced the orbital overlap between chromophores, resulting in negligible exchange and CT interactions. We also calculated excitonic coupling with a transition charge from the electrostatic potential (TrESP) method.[26,38] It is noted that the TrESP method can calculate only the Coulomb interaction. As also listed in Table I, the excitonic coupling value obtained with the TrESP method was 25.0 cm^{-1}, which was almost the same as the TDFI value (25.1 cm^{-1}). Therefore, it was found that the TrESP method is also applicable to the excitonic coupling calculation for KR2.

Subsequently, we performed the absorption and CD spectral calculations of the KR2 pentamer using the exciton model. As mentioned above, the SAC-CI excitation energy for the KR2 monomer (2.33 eV) was closer to the experimental value for the KR2 pentamer (2.37 eV[41]) than the TD-CAM-B3LYP value (2.82 eV). Therefore, the SAC-CI values were used to construct the Hamiltonian matrix. Figure 1(b) shows the pentamer structures used for the calculations. The intensities of the calculated spectra were given per monomer. As shown in Fig. 2(a), the calculated absorption spectrum of the KR2 pentamer exhibited a large positive band at 532 nm (2.33 eV). This peak position well reproduced the experimental values (524 nm, 2.37 eV) shown in Fig. 2(c). These results also showed that the peak position of the KR2 pentamer is almost the same as that of the monomer [Fig. 1(a)], while the intensity was higher than that of the monomer. Thus, we found that multimeric interactions had little effect on the peak position of the absorption spectrum.

The calculated CD spectrum of the pentamer is shown in Fig. 2(b), where a positive CD band is confirmed at 558 nm (2.22 eV). This peak position was in good agreement with the experimental value (544 nm, 2.28 eV) shown in Fig. 2(d). Although the calculated CD spectrum showed a slight negative band at 471 nm, the exciton model with TDFI could almost reproduce the shape and peak position of the experimental CD spectrum for the KR2 pentamer. It should be noted that the peak position for the pentamer (558 nm, 2.22 eV) was red-shifted by 26 nm (0.11 eV), compared with that for the monomer (532 nm, 2.33 eV). This result strongly suggested an effect of the multimeric interaction on the shape of the CD spectrum.

To investigate the dependence of the CD spectrum on the number of proteins, we also calculated the CD spectra of dimer, trimer, and tetramer of KR2 using the exciton model. It is noted that the CD spectrum of KR2 measured in the experiment is only for the pentamer. As shown in Fig. 3, all CD spectra of the dimer to the pentamer showed large positive bands, but different peak positions. This band was gradually red-shifted from 534 nm (the dimer) to 558 nm (the pentamer) with an increase in the number of proteins. Therefore, the multimerization of KR2 was found to affect the shape of the CD spectrum. Such a multimerization effect has not been experimentally observed in KR2, but the red shift of the CD spectrum due to the multimeric effect has been experimentally confirmed in *Gloeobacter* rhodopsin (GR).[66]

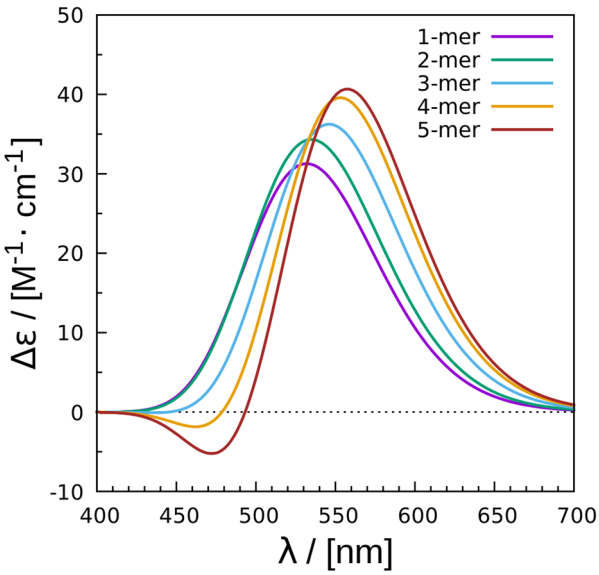

FIG. 3. Theoretical CD spectra of the KR2 monomer to pentamer. The values are given per monomer.

We further analyzed the CD components. Figure 4 shows the CD components of the KR2 dimer and the pentamer. All the spectra of the dimer to the pentamer were composed of positive and negative CD components. In the dimer spectrum, both one positive component and one negative component had high intensities, while in the pentamer spectra, two positive components and one negative component had higher intensities. In these spectra, the positive component appeared at longer wavelength than the negative component. These components canceled each other, resulting in a large positive CD band. As mentioned above, the pentamer CD band obtained with the exciton model was red-shifted by 26 nm, compared with the monomer band. This can be explained as follows. In the pentamer spectrum, the two positive CD components showed peaks (347 M^{-1} cm^{-1} and 231 M^{-1} cm^{-1}) at longer wavelength (532 nm) than the negative component (−555 M^{-1} cm^{-1} at 529 nm). Furthermore, the sum of the two positive CD components had a larger magnitude than the negative component. Thus, the cancellation of these components resulted in a spectral red shift in the overall CD spectrum (558 nm), compared to the original peak positions of the components (532 nm and 529 nm). From these analyses, we understood how the red shift of the CD spectrum occurs in the KR2 pentamer.

We also analyzed the reason why the positive CD component appears at a longer wavelength than the negative CD component. According to the exciton chirality method,[8,11] the sign of the dihedral angle when bringing the front transition dipole to the back transition dipole corresponds to the sign of the CD component at

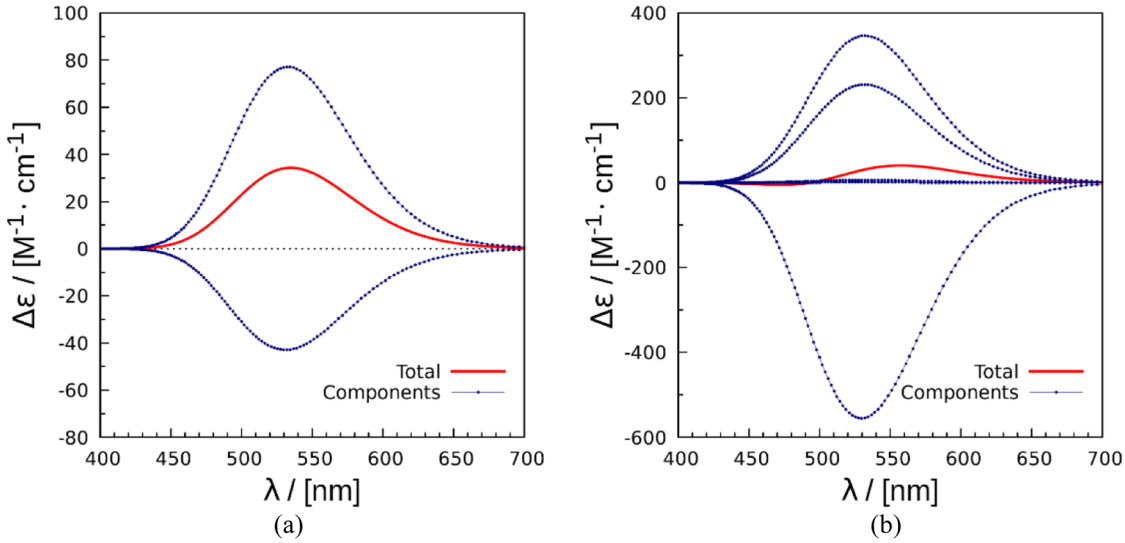

FIG. 4. Theoretical CD components of KR2: (a) dimer and (b) pentamer. The values are given per monomer.

a longer wavelength. Figure 5 shows two retinal chromophores in the KR2 pentamer. The red arrows represent the transition dipole moment of each retinal chromophore. This system clearly shows the clockwise rotation from the transition dipole of retinal *A* (front) to that of retinal *B* (back). Therefore, it was found that the positive rotational angle (the clockwise rotation) between the transition dipoles contributes significantly to the positive CD spectrum of KR2.

To investigate the effect of excitonic coupling, we also performed another type of spectral calculation, in which off-diagonal element values (i.e., excitonic coupling) were excluded from the Hamiltonian matrix. Hereinafter, this calculation is called a no-coupling model.[39] The absorption spectrum obtained with the no-coupling model exhibited a positive band at 532 nm (data not shown). This peak position did not shift from the result of the exciton model (532 nm). These results showed that the excitonic coupling hardly affected the absorption spectrum of the KR2 pentamer. In contrast, the CD spectrum obtained with the no-coupling model showed a different shape from that with the exciton model. The no-coupling model gave a CD band at 532 nm (data not shown), which did not show the red shift of the CD band as obtained with the exciton model (558 nm). Furthermore, the CD intensity was lower in the no-coupling model than in the exciton model. It is noted that the no-coupling model corresponds to the isolated chromophore calculation. Thus, the results clearly showed that the convolution of the separately calculated CD spectra for the individual chromophores failed to reproduce the experimental CD spectrum of the KR2 pentamer. From these results, we found that the excitonic coupling values in the Hamiltonian matrix significantly contribute to the CD spectral shape of the KR2 pentamer.

We further examined the dependence of the CD spectrum on the value of excitonic coupling. The excitonic coupling values of 10 cm^{-1}, 20 cm^{-1}, 30 cm^{-1}, 50 cm^{-1}, and 100 cm^{-1} were considered in the CD calculations. It is noted that these calculations used the same values as in Fig. 2(b), except for the excitonic coupling. The calculated CD spectrum is shown in Fig. 6. The intensities of the calculated spectra were given per monomer. For 10 cm^{-1}, the CD spectrum showed only a single positive band, while the spectrum gradually formed a negative band in addition to the positive band with an increase in the excitonic coupling values. The appearance of a distinct biphasic CD spectrum was confirmed above 30 cm^{-1}. These results clearly showed that the magnitude of the excitonic coupling has a significant effect on the shape of the CD spectrum. From these results, we could confirm that the weak excitonic coupling of about 20 cm^{-1} is important for the spectral red shift and the single positive band in the experimentally observed CD spectrum of KR2.

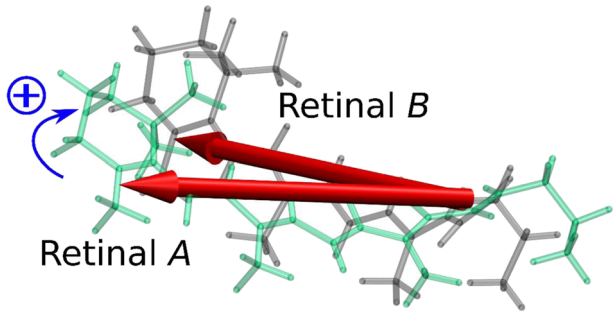

FIG. 5. Intermolecular conformation of two retinal chromophores (retinal *A* and retinal *B*) in KR2. The red arrows represent the transition dipole moment of each retinal chromophore.

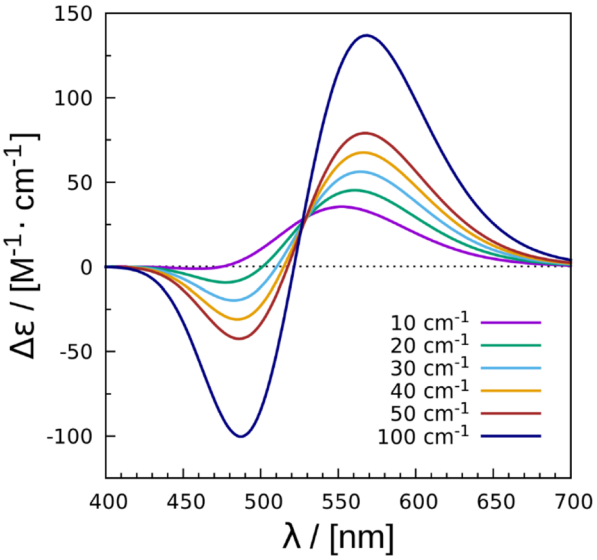

FIG. 6. CD spectra of the KR2 pentamer calculated with the exciton model using the excitonic coupling of 10 cm^{-1}, 20 cm^{-1}, 30 cm^{-1}, 40 cm^{-1}, 50 cm^{-1}, and 100 cm^{-1}. The values are given per monomer.

V. CONCLUSIONS

In this paper, we investigated the excitonic coupling effect on the CD spectrum of the KR2 pentamer using the exciton model combined with the TDFI method. The TDFI method allows for an accurate description and detailed analysis of excitonic coupling, in terms of Coulomb, exchange, and CT interactions. Taking advantage of this benefit, we investigated the major contributions to excitonic coupling. The results of this study clearly showed a dominant contribution of the Coulomb interaction to the excitonic coupling value. In contrast, the exchange and CT interactions resulted in negligible contributions. The results also indicated that EET between retinal chromophores is less likely to occur in KR2 because of the small magnitude of excitonic coupling (25.1 cm^{-1}). The excitonic coupling values were employed for the spectral calculations with the exciton model. As a result, the main features of the experimental absorption and CD spectra of KR2 were successfully reproduced. Based on these results, we explored the mechanism of the CD spectral shape observed in the KR2 pentamer. As a result of the analysis, the excitonic coupling between retinal chromophores was found to be indispensable for the quantitative description of the red-shifted CD band compared to the monomer spectrum. Further analysis revealed that the weak excitonic coupling of about 20 cm^{-1} plays a crucial role in the single positive CD band of KR2.

This is the first computational study on the CD spectrum of KR2. The findings of this study provide the basis for understanding the origin of the KR2 CD spectrum. The exciton model combined with TDFI used in this study is a promising approach for calculating CD spectra. Although the QM/MM calculation based on the SAC-CI method for the KR2 pentamer is not realistic due to the huge computational cost, the exciton model combined with TDFI enables the CD calculation based on the SAC-CI method. Furthermore, the present approach can be combined with other electronic structure methods. The high accuracy and broad applicability of the exciton model combined with TDFI are useful for analyzing the molecular mechanisms underlying the chromophore–chromophore interactions in biological molecular aggregates.

ACKNOWLEDGMENTS

This study was supported by JSPS KAKENHI Grant Nos. 16K05670 and 20K05430 (to K.J.F.) and Grant No. 17H03007 (to K.I.).

DATA AVAILABILITY

The data that support the findings of this study are available from the corresponding author upon reasonable request.

REFERENCES

[1]N. Berova, K. Nakanishi, and R. W. Woody, *Circular Dichroism: Principles and Applications*, 2nd ed. (Wiley VCH, New York, 2000).
[2]C. A. Hasselbacher, J. L. Spudich, and T. G. Dewey, "Circular dichroism of halorhodopsin: Comparison with bacteriorhodopsin and sensory rhodopsin I," Biochemistry **27**, 2540–2546 (1988).
[3]J. Y. Cassim, "Unique biphasic band shape of the visible circular dichroism of bacteriorhodopsin in purple membrane," Biophys. J. **63**, 1432–1442 (1992).
[4]C. M. Davis, P. L. Bustamante, and P. A. Loach, "Reconstitution of bacterial core light-harvesting complexes of *Rhodobacter sphaeroides* and *Rhodospirillum rubrum* with isolated α- and β-polypeptides, bacteriochlorophyll *a*, and carotenoid," J. Biol. Chem. **270**, 5793–5804 (1995).
[5]S. Georgakopoulou, R. van Grondelle, and G. van der Zwan, "Circular dichroism of carotenoids in bacterial light-harvesting complexes: Experiments and modeling," Biophys. J. **87**, 3010–3022 (2004).
[6]J. Adolphs, F. Müh, M. E.-A. Madjet, M. S. am Busch, and T. Renger, "Structure-based calculations of optical spectra of photosystem I suggest an asymmetric light-harvesting," J. Am. Chem. Soc. **132**, 3331–3343 (2010).
[7]G. Pescitelli and R. W. Woody, "The exciton origin of the visible circular dichroism spectrum of bacteriorhodopsin," J. Phys. Chem. B **116**, 6751–6763 (2012).
[8]N. Harada and K. Nakanishi, *Circular Dichroic Spectroscopy: Exciton Coupling in Organic Stereochemistry* (University Science Books, Mill Valley, CA, 1983).
[9]I. Tinoco, Jr., "Theoretical aspects of optical activity," Adv. Chem. Phys. **4**, 113–160 (1962).
[10]R. W. Woody, "Improved calculation of the $n\pi^*$ rotational strength in polypeptides," J. Chem. Phys. **49**, 4797–4806 (1968).
[11]N. Harada and K. Nakanishi, "Determining the chiralities of optically active glycols," J. Am. Chem. Soc. **91**, 3989–3991 (1969).
[12]P. M. Bayley, E. B. Nielsen, and J. A. Schellman, "Rotatory properties of molecules containing two peptide groups: Theory," J. Phys. Chem. **73**, 228–243 (1969).
[13]W. J. Goux and T. M. Hooker, Jr., "Chiroptical properties of proteins. I. Near-ultraviolet circular dichroism of ribonuclease S," J. Am. Chem. Soc. **102**, 7080–7087 (1980).
[14]J. D. Hirst, "Improving protein circular dichroism calculations in the far-ultraviolet through reparametrizing the amide chromophore," J. Chem. Phys. **109**, 782–788 (1998).
[15]N. A. Besley and J. D. Hirst, "Theoretical studies toward quantitative protein circular dichroism calculations," J. Am. Chem. Soc. **121**, 9636–9644 (1999).
[16]N. Sreerama and R. W. Woody, "Computation and analysis of protein circular dichroism spectra," Methods Enzymol. **383**, 318–351 (2004).
[17]W. Kuhn, "The physical significance of optical rotatory power," Trans. Faraday Soc. **26**, 293–308 (1930).

[18]J. G. Kirkwood, "On the theory of optical rotatory power," J. Chem. Phys. **5**, 479–491 (1937).
[19]J. Frenkel, "On the transformation of light into heat in solids. II," Phys. Rev. **37**, 1276–1294 (1931).
[20]J. C. Chang, "Monopole effects on electronic excitation interactions between large molecules. I. Application to energy transfer in chlorophylls," J. Chem. Phys. **67**, 3901–3909 (1977).
[21]B. P. Krueger, G. D. Scholes, and G. R. Fleming, "Calculation of couplings and energy-transfer pathways between the pigments of LH2 by the ab initio transition density cube method," J. Phys. Chem. B **102**, 5378–5386 (1998).
[22]S. Tretiak, C. Middleton, V. Chernyak, and S. Mukamel, "Exciton Hamiltonian for the bacteriochlorophyll system in the LH2 antenna complex of purple bacteria," J. Phys. Chem. B **104**, 4519–4528 (2000).
[23]C.-P. Hsu, G. R. Fleming, M. Head-Gordon, and T. Head-Gordon, "Excitation energy transfer in condensed media," J. Chem. Phys. **114**, 3065–3072 (2001).
[24]M. F. Iozzi, B. Mennucci, J. Tomasi, and R. Cammi, "Excitation energy transfer (EET) between molecules in condensed matter: A novel application of the polarizable continuum model (PCM)," J. Chem. Phys. **120**, 7029–7040 (2004).
[25]K. F. Wong, B. Bagchi, and P. J. Rossky, "Distance and orientation dependence of excitation transfer rates in conjugated systems: Beyond the Förster theory," J. Phys. Chem. A **108**, 5752–5763 (2004).
[26]M. E. Madjet, A. Abdurahman, and T. Renger, "Intermolecular Coulomb couplings from *ab initio* electrostatic potentials: Application to optical transitions of strongly coupled pigments in photosynthetic antennae and reaction centers," J. Phys. Chem. B **110**, 17268–17281 (2006).
[27]J. Neugebauer, "Couplings between electronic transitions in a subsystem formulation of time-dependent density functional theory," J. Chem. Phys. **126**, 134116 (2007).
[28]B. Fückel, A. Köhn, M. E. Harding, G. Diezemann, G. Hinze, T. Basché, and J. Gauss, "Theoretical investigation of electronic excitation energy transfer in bichromophoric assemblies," J. Chem. Phys. **128**, 074505 (2008).
[29]R. F. Fink, J. Pfister, H. M. Zhao, and B. Engels, "Assessment of quantum chemical methods and basis sets for excitation energy transfer," Chem. Phys. **346**, 275–285 (2008).
[30]J. Vura-Weis, M. D. Newton, M. R. Wasielewski, and J. E. Subotnik, "Characterizing the locality of diabatic states for electronic excitation transfer by decomposing the diabatic coupling," J. Phys. Chem. C **114**, 20449–20460 (2010).
[31]T. Kawatsu, K. Matsuda, and J. Hasegawa, "Bridge-mediated excitation energy transfer pathways through protein media: A slater determinant-based electronic coupling calculation combined with localized molecular orbitals," J. Phys. Chem. A **115**, 10814–10822 (2011).
[32]A. A. Voityuk, "Estimation of electronic coupling for photoinduced charge separation and charge recombination using the fragment charge difference method," J. Phys. Chem. C **117**, 2670–2675 (2013).
[33]K. J. Fujimoto, "Electronic coupling calculations with transition charges, dipoles, and quadrupoles derived from electrostatic potential fitting," J. Chem. Phys. **141**, 214105 (2014).
[34]B. Błasiak, M. Maj, M. Cho, and R. W. Góra, "Distributed multipolar expansion approach to calculation of excitation energy transfer couplings," J. Chem. Theory Comput. **11**, 3259–3266 (2015).
[35]K. J. Fujimoto and S. Hayashi, "Electronic Coulombic coupling of excitation-energy transfer in xanthorhodopsin," J. Am. Chem. Soc. **131**, 14152–14153 (2009).
[36]K. J. Fujimoto, "Transition-density-fragment interaction combined with transfer integral approach for excitation-energy transfer via charge-transfer states," J. Chem. Phys. **137**, 034101 (2012).
[37]K. J. Fujimoto, in *Chemical Science of π-Electron Systems*, edited by T. Akasaka, A. Osuka, S. Fukuzumi, H. Kandori, and Y. Aso (Springer, Tokyo, Japan, 2015), pp. 761–777.
[38]K. J. Fujimoto, "Transition-density-fragment interaction approach for exciton-coupled circular dichroism spectra," J. Chem. Phys. **133**, 124101 (2010).
[39]K. J. Fujimoto and S. P. Balashov, "Vibronic coupling effect on circular dichroism spectrum: Carotenoid–retinal interaction in xanthorhodopsin," J. Chem. Phys. **146**, 095101 (2017).
[40]K. J. Fujimoto and C. Kitamura, "A theoretical study of crystallochromy: Spectral tuning of solid-state tetracenes," J. Chem. Phys. **139**, 084511 (2013).
[41]K. Inoue, H. Ono, R. Abe-Yoshizumi, S. Yoshizawa, H. Ito, K. Kogure, and H. Kandori, "A light-driven sodium ion pump in marine bacteria," Nat. Commun. **4**, 1678 (2013).
[42]H. E. Kato, K. Inoue, R. Abe-Yoshizumi *et al.*, "Structural basis for Na^+ transport mechanism by a light-driven Na^+ pump," Nature **521**, 48–53 (2015).
[43]I. Gushchin, V. Shevchenko, V. Polovinkin *et al.*, "Crystal structure of a light-driven sodium pump," Nat. Struct. Mol. Biol. **22**, 390–395 (2015).
[44]K. Inoue, M. Konno, R. Abe-Yoshizumi, and H. Kandori, "The role of the NDQ motif in sodium-pumping rhodopsins," Angew. Chem., Int. Ed. **54**, 11536–11539 (2015).
[45]H. Kandori, K. Inoue, and S. P. Tsunoda, "Light-driven sodium-pumping rhodopsin: A new concept of active transport," Chem. Rev. **118**, 10646–10658 (2018).
[46]K. Deisseroth, G. Feng, A. K. Majewska, G. Miesenbock, A. Ting, and M. J. Schnitzer, "Next-generation optical technologies for illuminating genetically targeted brain circuits," J. Neurosci. **26**, 10380–10386 (2006).
[47]Y. I. Wu, D. Frey, O. I. Lungu, A. Jaehrig, I. Schlichting, B. Kuhlman, and K. M. Hahn, "A genetically encoded photoactivatable Rac controls the motility of living cells," Nature **461**, 104–108 (2009).
[48]E. S. Koganov, V. Brumfeld, N. Friedman, and M. Sheves, "Origin of circular dichroism of xanthorhodopsin. A study with artificial pigments," J. Phys. Chem. B **119**, 456–464 (2015).
[49]M. Shibata, K. Inoue, K. Ikeda, M. Konno, M. Singh, C. Kataoka, R. Abe-Yoshizumi, H. Kandori, and T. Uchihashi, "Oligomeric states of microbial rhodopsins determined by high-speed atomic force microscopy and circular dichroic spectroscopy," Sci. Rep. **8**, 8262 (2018).
[50]P. -O. Löwdin, "On the non-orthogonality problem connected with the use of atomic wave functions in the theory of molecules and crystals," J. Chem. Phys. **18**, 365–375 (1950).
[51]A. Warshel and M. Levitt, "Theoretical studies of enzymic reactions: Dielectric, electrostatic and steric stabilization of the carbonium ion in the reaction of lysozyme," J. Mol. Biol. **103**, 227–249 (1976).
[52]W. Kohn and L. J. Sham, "Self-consistent equations including exchange and correlation effects," Phys. Rev. **140**, A1133 (1965).
[53]C. Lee, W. Yang, and R. G. Parr, "Development of the Colle–Salvetti correlation-energy formula into a functional of the electron density," Phys. Rev. B **37**, 785–789 (1988).
[54]J. Wang, P. Cieplak, and P. A. Kollman, "How well does a restrained electrostatic potential (RESP) model perform in calculating conformational energies of organic and biological molecules?," J. Comput. Chem. **21**, 1049–1074 (2000).
[55]K. Fujimoto and W. Yang, "Density-fragment interaction approach for quantum-mechanical/molecular-mechanical calculations with application to the excited states of a Mg^{2+}-sensitive dye," J. Chem. Phys. **129**, 054102 (2008).
[56]H. Nakatsuji, "Cluster expansion of the wavefunction. Excited states," Chem. Phys. Lett. **59**, 362–364 (1978).
[57]E. Runge and E. K. U. Gross, "Density-functional theory for time-dependent systems," Phys. Rev. Lett. **52**, 997–1000 (1984).
[58]T. Yanai, D. P. Tew, and N. C. Handy, "A new hybrid exchange–correlation functional using the Coulomb-attenuating method (CAM-B3LYP)," Chem. Phys. Lett. **393**, 51–57 (2004).
[59]H. M. Senn and W. Thiel, "QM/MM methods for biomolecular systems," Angew. Chem., Int. Ed. **48**, 1198–1229 (2009).
[60]J. W. Ponder, *Tinker4.2* (Washington University, St. Louis, MO, 2004).
[61]M. J. Frisch, G. W. Trucks, H. B. Schlegel *et al.*, Gaussian09, Revision A.02, Gaussian, Inc., Wallingford, CT, 2009.
[62]S. P. Balashov, E. S. Imasheva, V. A. Boichenko, J. Antón, J. M. Wang, and J. K. Lanyi, "Xanthorhodopsin: A proton pump with a light-harvesting carotenoid antenna," Science **309**, 2061–2064 (2005).

[63]S. P. Balashov, E. S. Imasheva, and J. K. Lanyi, "Induced chirality of the light-harvesting carotenoid salinixanthin and its interaction with the retinal of xanthorhodopsin," Biochemistry **45**, 10998–11004 (2006).
[64]T. Polívka, S. P. Balashov, P. Chábera, E. S. Imasheva, A. Yartsev, V. Sundström, and J. K. Lanyi, "Femtosecond carotenoid to retinal energy transfer in xanthorhodopsin," Biophys. J. **96**, 2268–2277 (2009).
[65]G. D. Scholes, R. D. Harcourt, and K. P. Ghiggino, "Rate expressions for excitation transfer. III. An *ab initio* study of electronic factors in excitation transfer and exciton resonance interactions," J. Chem. Phys. **102**, 9574–9581 (1995).
[66]T. Tsukamoto, T. Kikukawa, T. Kurata, K.-H. Jung, N. Kamo, and M. Demura, "Salt bridge in the conserved His-Asp cluster in *Gloeobacter* rhodopsin contributes to trimer formation," FEBS Lett. **587**, 322–327 (2013).